

Impact of Tidal Energy Converter (TEC) Array Operation on Sediment Dynamics

Simon P. Neill* and Scott J. Couch†

* *School of Ocean Sciences, Bangor University
Menai Bridge, UK*

s.p.neill@bangor.ac.uk

† *Institute for Energy Systems, The University of Edinburgh
Edinburgh, UK*

scott.couch@ed.ac.uk

Abstract—Large-scale exploitation of the tidal stream resource is likely to alter the regional hydrodynamics, but for practical extraction scenarios this effect is generally considered to be very small. However, since sediment transport is proportional to the cube of velocity, relatively small changes in the tidal currents could translate into large changes in the sediment dynamics. Here, we investigate this effect in relation to two oceanographic processes: tidal asymmetry and headland sand bank maintenance. Both of these processes have major practical significance. Tidal symmetry/asymmetry is responsible for the large-scale long-term distribution of shelf sea sediment. Any tidal energy scheme which has the potential to alter this large-scale distribution could affect the supply of sediment feeding into natural coastal defence systems which remove energy from storm waves, such as beaches and offshore sand banks. Headlands are some of the most attractive regions for exploitation of the tidal stream resource. Any tidal energy scheme which could lead to changes in the morphodynamics of the associated headland sand banks could have implications for coastal flooding, due to changes in the wave distribution, including wave refraction and depth-induced wave breaking.

Index Terms—Tidal energy converter, tidal stream turbines, energy extraction, sediment dynamics, sand banks, tidal symmetry, Bristol Channel

I. INTRODUCTION

Tidal energy converter (TEC) devices operate by intercepting the kinetic energy in strong tidal currents (typically through a turbine unit). This intercepted energy is then converted to electrical energy through a power take-off system (e.g. an induction generator) and conditioned for dispatch to the electricity network. Theoretically, this is similar to the operation of a typical wind energy device. However, what is significantly different from the wind energy analogy is the environment that TEC devices operate in [1], and the potential for TEC devices to interact with their environment [2]. Although the key environmental variables likely to be impacted by TEC device operation have long been identified (e.g. collision risk, acoustic emissions, sediment dynamics and morphodynamics) [3], few of these impacts have yet been quantified [4]. This lack of progress is potentially slowing down the commercialisation and full-scale exploitation of the tidal stream resource.

Extracting energy from a tidal system will result in changes to the velocity structure, including an overall reduction in

current speed over the larger area domain [2]. This reduction in current speed, even for relatively large TEC array extraction scenarios, is generally quite small. For example, in a tidal channel the impact of energy extraction on current speed U becomes noticeable only when the energy extracted reaches around 10% of the available kinetic energy flux [5], a considerably large amount of energy to extract from a channel. More realistic extraction scenarios (typically 1% of the available kinetic energy) could therefore be perceived to have very little environmental impact. However, bed shear stress is a function of U^2 . Therefore, small changes in the tidal currents could potentially lead to large changes in the resulting bed shear stress. Further, the transport of sediments is proportional to an even higher power of velocity than bed shear stress, e.g. total load transport by currents (bedload and suspended load) is a function of $U^{3.4}$ [6]. Therefore, relatively small changes to the residual flow field caused by exploitation of the tidal stream resource could have a significant influence on the residual sediment transport pathways.

Generally, sites suitable for TEC arrays are selected based on technical (e.g. water depth) and economic (e.g. mean kinetic power density) constraints (e.g. [7]). This research considers additional criteria which, if not addressed, could lead to negative environmental impacts. We examine the effects of TEC array operation on sediment dynamics and morphodynamics, with respect to two classical oceanographic processes: tidal asymmetry and headland sand bank maintenance.

II. TIDAL ASYMMETRY AND ENERGY EXTRACTION

Pingree and Griffiths [8] noted that the mean bed shear stress distributions associated with the principal lunar semi-diurnal (M_2) and quarter-diurnal (M_4) tides tend to be directed into bays and to diverge from M_2 amphidromic points, reaching maximum values at M_4 amphidromic points. They further suggested that the interaction between the M_2 and M_4 tides determines the direction of net sand transport around the British Isles. Regions of modelled bed stress divergence compared favourably with sediment bed load partings, based on observations of the seabed sediment composition around the British Isles [9] and in the Irish Sea [10], [11].

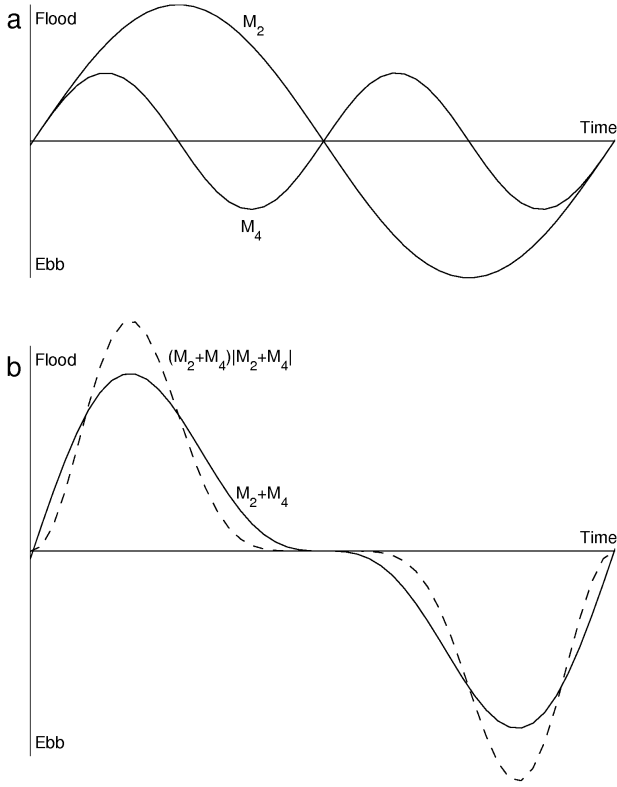


Fig. 1. Combination of M_2 and M_4 tidal currents resulting in tidal symmetry. (a) Tidal currents for individual constituents and (b) tidal currents (solid line) and bed stress (dashed line) resulting from superposition of M_2 and M_4 constituents. Based on [8].

It is the phase relationship between the M_2 and M_4 tidal currents that leads to asymmetry [8], [12]. Although the combination of M_2 and M_4 tidal currents in Fig. 1a results in a distorted tide (Fig. 1b), the flood and ebb tides are equal in magnitude, as is the bed shear stress (based here on the assumption of a quadratic friction law). Hence, there is no residual sediment transport. By combining M_2 and M_4 tidal currents as in Fig. 2a, however, the flood tide is stronger than the ebb (Fig. 2b). Although there is no net residual flow, the integrated square of the velocity (U^2) is greater during the flood. Hence, there is a residual bed shear stress and the net direction of sediment transport will be in the flood direction. In the case where the flood and ebb currents are equal

$$2\phi_{M_2} = \phi_{M_4} + 90^\circ \quad (1)$$

and where there is a maximum asymmetry

$$2\phi_{M_2} = \phi_{M_4} \quad (2)$$

where ϕ_{M_2} and ϕ_{M_4} are the phases (in degrees) of the M_2 and M_4 tidal currents, respectively. Hence, a plot of $2\phi_{M_2} - \phi_{M_4}$ quantifies tidal asymmetry, demonstrated in Fig. 3a for the tidal mean bed stress, $\bar{\tau}_0$. Since bed level change is related to the divergence of the tidal residual bed shear stress, for 1D flow a plot of $-\partial\bar{\tau}_0/\partial x$ can be used to infer

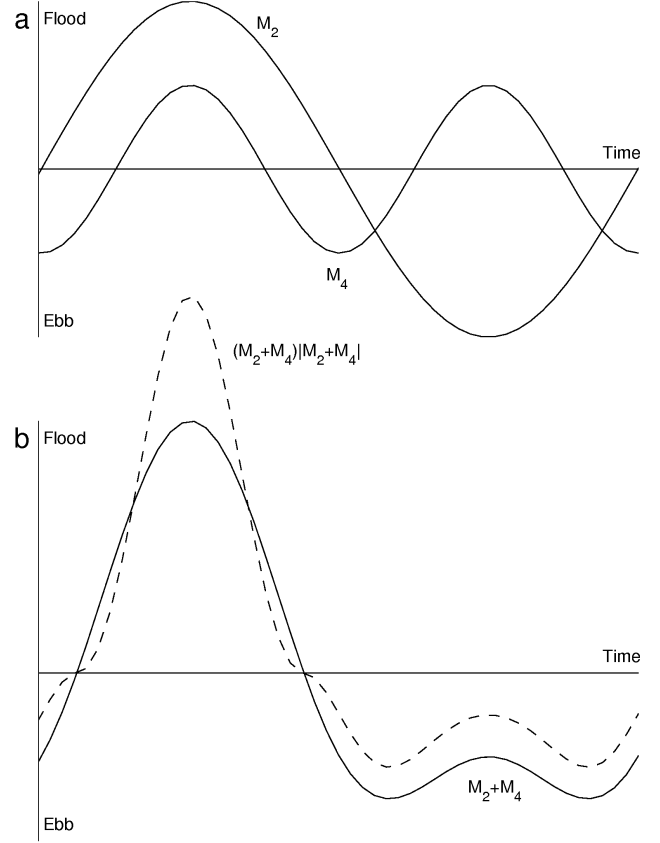


Fig. 2. Combination of M_2 and M_4 tidal currents resulting in tidal asymmetry. (a) Tidal currents for individual constituents and (b) tidal currents (solid line) and bed stress (dashed line) resulting from superposition of M_2 and M_4 constituents. Based on [8].

bed level change for spatial changes in $2\phi_{M_2} - \phi_{M_4}$ (Fig. 3b). Sediment will accumulate (i.e. positive bed level change) in regions of bed shear stress convergence ($\partial\bar{\tau}_0/\partial x < 0$) whereas sediment will be eroded from regions of bed shear stress divergence ($\partial\bar{\tau}_0/\partial x > 0$). Zero bed level change occurs in regions of maximum asymmetry (0° and 180°) whereas regions of symmetry (90° and 270°) are associated with the maximum magnitude of bed level change (since regions of tidal symmetry are either regions of sediment convergence or divergence).

When energy is extracted from a tidal system which exhibits varying magnitudes of tidal asymmetry, the effect on residual bed stress and the corresponding bed level change can be considered. In regions of tidal symmetry (90° and 270° in Fig. 3), energy extraction will have no influence on the large-scale morphodynamics of a tidal system since the residual bed stress is unaltered. In regions of maximum tidal asymmetry (0° and 180°), energy extraction is expected to have a maximum impact on the large-scale morphodynamics of a tidal system. In a relatively long tidal channel, different phase relationships between the M_2 and M_4 tidal currents will occur. The Bristol Channel, for example, has well-documented

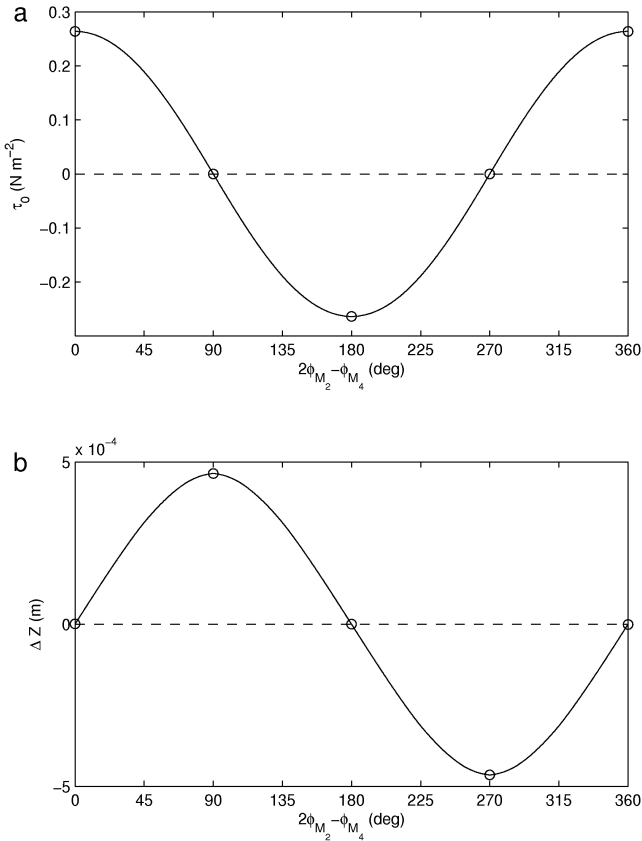


Fig. 3. Tidal residual bed stress and associated bed level change resulting from varying phase relationships between the M_2 and M_4 tidal currents. Maximum tidal asymmetry and hence zero bed level change occurs at 0° and 180° . Tidal symmetry and hence maximum bed level change occurs at 90° and 270° . (a) Tidal residual bed stress and (b) bed level change. These calculations are based on tidal current amplitudes of 1.0 and 0.25 m s^{-1} for the M_2 and M_4 constituents, respectively, and $C_D = 0.0025$.

bed-stress divergence and convergence zones, which have been related to sediment transport and morphodynamics [11]. The hypothesis to be tested here is that in such a channel, energy extracted from regions of tidal asymmetry will have a much greater influence on sediment dynamics than energy extracted from regions of tidal symmetry.

A. Case Study: The Bristol Channel

The Bristol Channel (Fig. 4) separates South Wales from South West England and extends from the lower estuary of the River Severn to the Celtic Sea. For the purposes of this paper, however, the term Bristol Channel is taken to include the Severn Estuary. Depths in the outer region of the Bristol Channel are around 50 m, and an extensive system of narrow channels and tidal flats in the upper part of the estuary reduces the depth to less than 10 m upstream of Newport. With a mean spring range of 12.2 m and a mean neap range of 6.0 m at Avonmouth, the Bristol Channel has one of the highest semi-diurnal ranges in the world. From tidal analysis, the dominant constituents in the Bristol Channel are M_2 and S_2 , but there is also a significant contribution from the M_4

constituent [13]. The amplitudes of the S_2 and M_4 constituents at Avonmouth are 36% and 6%, respectively, of the M_2 . The interference of reflected and incoming tides in the Bristol Channel produces a partially progressive wave, with a phase difference between elevation and currents close to that for a standing wave [14]. A well known sediment bed load parting zone exists in the Bristol Channel to the west of Hinkley Point [11]. Numerical models that can accurately predict tidal asymmetry are crucial to the understanding of such zones, and hence for understanding large scale sediment dynamics.

There has been much speculation on the harvesting of tidal energy in the Bristol Channel. Most prominent are various tidal barrage schemes designed to capitalise on the energy resource contained in the large tidal range (e.g. [15]). Alternate tidal lagoon projects have also been proposed (e.g. [16]). In terms of the tidal stream resource, the Bristol Channel has been identified as accounting for around 2% of the total UK ‘extractable’ resource [17]. Although no large scale commercial scheme has yet been proposed for the area, Marine Current Turbines (MCT) installed a 300 kW rated experimental tidal stream turbine in the Bristol Channel, to the west of Hinkley Point. This test device, known as ‘Seaflow’, was operational in the years 2003-2009. In addition to the extreme tidal range and fast tidal currents in the Bristol Channel, the characteristics of the National Grid in the region are also encouraging for the development of new energy generation solutions. In most regions of the UK, the development of renewable energy is constrained by the lack of capacity available on the existing grid infrastructure. The south-west has been identified as a region of the UK where spare capacity currently exists both at the distribution and transmission level [18].

B. One-Dimensional Morphological Model

To test the hypothesis outlined above, a one-dimensional (1D) morphological model was developed and applied to the Bristol Channel, where large spatial variations in tidal asymmetry occur along the length of the channel. Previous studies have demonstrated that 1D models of the Bristol Channel are appropriate for reproducing the main features of the hydrodynamics [13], [19], [20]. The morphological model consisted of three components: hydrodynamic, sediment transport and bed level change models. The model is described fully in [21], hence only the governing equations and key points are included here.

Longitudinal variations in the time-varying free surface and velocity were calculated using the 1D sectionally-averaged continuity equation

$$\frac{\partial \eta}{\partial t} = -\frac{1}{B} \frac{\partial(AU)}{\partial x} \quad (3)$$

and momentum equation

$$\frac{\partial U}{\partial t} = -g \frac{\partial \eta}{\partial x} - \frac{C_D U |U|}{(h + \eta)^{4/3}} - \frac{P_x}{\rho U \delta x B (h + \eta)} \quad (4)$$

where η is the variation of the free surface from mean sea level, B is the channel width, A is the cross-sectional area of the

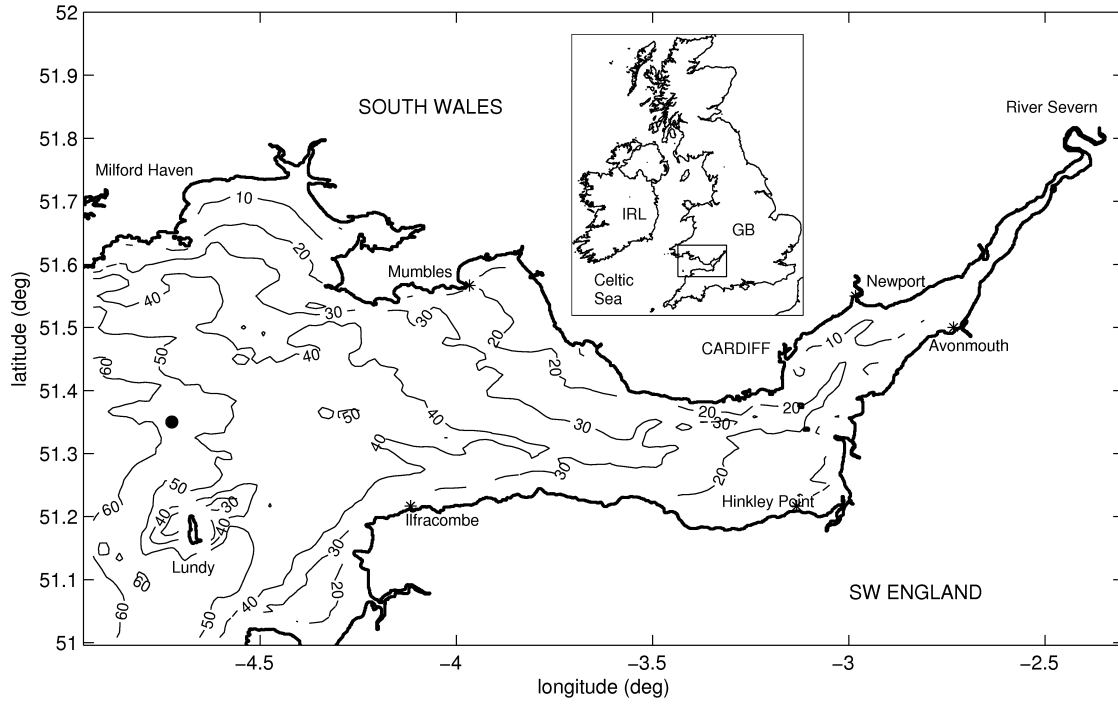


Fig. 4. Location and bathymetry of the Bristol Channel. Contours are depths in metres relative to mean sea level and the filled circle north of Lundy is the offshore boundary of the one-dimensional morphological model.

channel, U is the depth-averaged velocity, C_D is the bottom friction coefficient, h is the mean water depth, ρ is water density, δx is the model grid spacing and g is gravitational acceleration. The final term in Eq. 4 is the energy extraction term, with power extracted (P_x in Watts per grid point in the longitudinal direction) given as a function of current speed. The variation in the relationship between the power extracted and intercepted current speed is dependent upon the performance of the TEC technology adopted. As no device has yet reached commercialisation, the performance of individual devices is still the subject of development and debate. Douglas et al. have outlined basic technical specifications for a MCT ‘Seagen’ device [22]. Seagen is one of the more advanced technologies currently undergoing pre-commercialisation testing. Using the data provided in [22], the power curve presented in Fig. 5 was produced, based on the simplifying assumption of constant efficiencies across the performance range, and extending the rated velocity to 2.7 m s^{-1} to produce a 1.5 MW rated device (a Seagen device has two rotors). This is an idealised representation of the potential performance of a TEC device, and is not expected to be wholly realistic - for instance, it would be desirable from a techno-economic perspective for the power coefficient (C_p) curve to reach a maximum below, rather than at, the rated velocity. At velocities below the cut-in speed, the turbine does not generate sufficient lift to rotate the drive train. At velocities which exceed the rated speed of the turbine, power output is constant. Since the energy extraction term is proportional to U^2 , it is analogous to an additional bottom friction term [5].

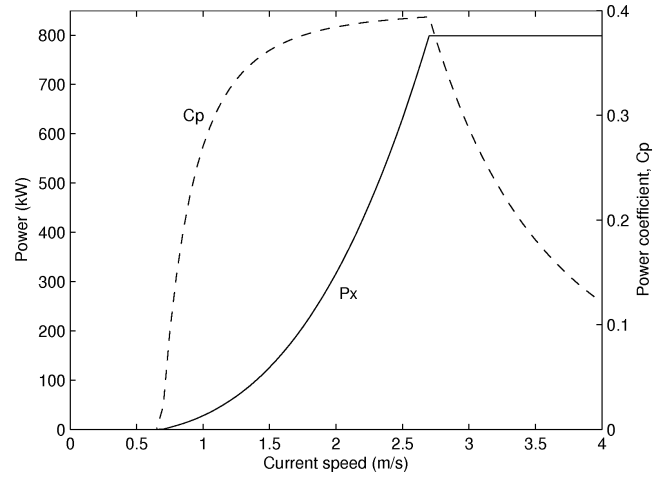


Fig. 5. Idealised power curve per rotor used to parameterise energy extraction in numerical model (based on [22]).

Total instantaneous (bedload plus suspended load) sediment transport was calculated using the Soulsby-Van Rijn transport formulation [6]. 1D morphological development of the channel in the x -direction was modelled using (e.g. [23])

$$\frac{\partial z}{\partial t} = -\frac{1}{1-p} \left\{ \frac{\partial q_t}{\partial x} \right\} \quad (5)$$

where z is the bed level and p is the bed porosity. The assumption was made that the bed was fully erodible for all

values of x .

C. Model Parameterisation

The morphological model was applied to a 155 km reach of the Bristol Channel, extending from an offshore location north of Lundy ($x = 0$) to the tidal limit (Fig. 4 and Fig. 6). The mean water depth and channel widths were extracted from a bathymetry dataset of the Irish and Celtic Seas which has a raw resolution of approximately 1 km [24]. This data was interpolated onto a longitudinal model grid spacing of $\delta x = 3167$ m (since the 155 km domain was divided into 49 cells, i.e. the model used 50 elevation points). The offshore model boundary was driven by elevation, using the M_2 , S_2 and M_4 astronomical constituents extracted from an existing three-dimensional tidal model of the Irish Sea [25]. The S_2 constituent was included to simulate more realistic velocity magnitudes than the M_2 and M_4 constituents would have provided alone, and to include non-linear effects due to combining the dominant tidal constituents. However, since the model output was examined after an integer number of spring/neap cycles, the combination of M_2 and S_2 constituents did not contribute to tidal asymmetry (the M_4 contribution served this purpose). The upstream model boundary (at the tidal limit) was reflective. Detailed validation of the hydrodynamics is provided in [21], in terms of the amplitudes and phases of the M_2 , S_2 and M_4 constituents at three locations along the channel. For such a relatively simple hydrodynamic model, the validation was very good, with mean errors of 13.6% in amplitude and 2.7% in phase.

To estimate the number of rotors (n) and the number of model grid cells required to accommodate a full-scale TEC array, the idealised power curve (Fig. 5) was used to parameterise the individual elements of a 250 MW tidal stream farm (approximately 168 devices, hence $n = 336$). Other than the availability of suitable tidal currents, practical/economic limitations restrict the exploitable resource available such as water depths in the range 25-45 m [1], and a minimum longitudinal turbine spacing of 15 device widths to reduce wake effects [26]. The overall (tip-to-tip) width of a Seagen device is 43 m, also used as the lateral spacing between devices. Hence, with a simple 12×14 rectangular array arrangement (number of longitudinal by lateral elements), this equates to a turbine farm with overall dimensions of 7568 m by 1161 m. Since the model grid spacing was 3167 m, power extraction for a 250 MW tidal stream farm can be represented by 168 Seagen devices distributed uniformly over 3 model grid cells.

The model was applied with a sediment median grain size of $d_{50} = 330$ μm (medium sand), based on in situ sampling over a large region of the estuary [27].

D. Model Results

The morphological model was applied to several simulations, each of duration 29.53 days (a lunar month) in order to remove any asymmetrical effects due to the combination of M_2 and S_2 constituents, assuming that the dynamics are

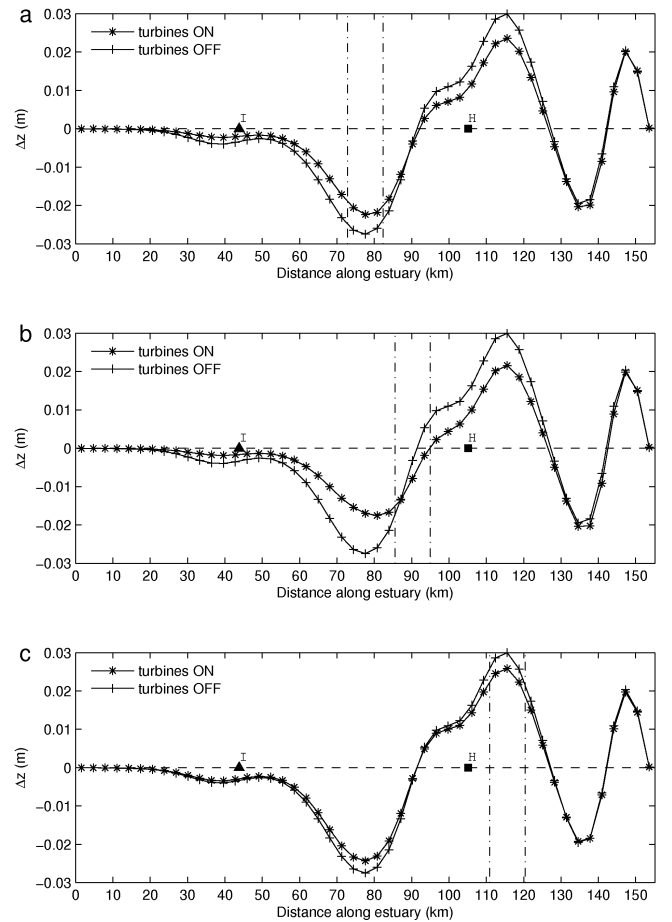


Fig. 6. Modelled bed level change after 29.53 days without and with a tidal stream farm placed at various locations along the channel. Vertical dash-dot lines show the longitudinal limits of each tidal stream farm. The filled triangle labelled I is the location of Ilfracombe, and the filled square labelled H is the location of Hinkley. (a) Tidal stream farm in region of sediment divergence (tidal symmetry), (b) tidal stream farm in region of tidal asymmetry and (c) tidal stream farm in region of sediment convergence (tidal symmetry).

largely linear. Initially, the power extraction term in Eq. 4 was switched off to provide a background bed level change over the modelled time period for a natural tidal channel. This resulted in maximum changes in bed level of magnitude 0.03 m (Fig. 6), corresponding with a diffuse zone of sediment divergence (bed load parting) between Ilfracombe and Hinkley ($x = 78$ km) and a diffuse zone of sediment convergence upstream of Hinkley ($x = 116$ km). Between these two regions of tidal symmetry was a zone of maximum tidal asymmetry ($x = 92$ km), where the net change in bed level was zero (compare with Fig. 3). Following this background simulation, energy was extracted from three strategic locations along the channel: a 250 MW tidal stream farm was centered on a region of sediment divergence (Fig. 6a), on a region of strong tidal asymmetry (Fig. 6b) and on a region of sediment convergence (Fig. 6c).

The results demonstrate that, regardless of the location of energy extraction, the magnitude of bed level change is damp-

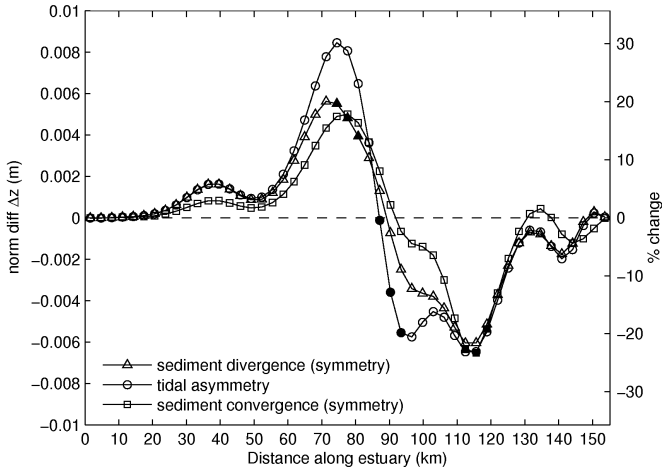


Fig. 7. Difference in bed level between turbine cases and non-turbine case, normalised by the gross mean sediment transport averaged over the duration of the simulation (Q_T). Filled symbols indicate model cells which contain tidal stream turbines for each case.

ened by the presence of a tidal stream farm (due to a general reduction in tidal velocity and hence net sediment transport). However, the location of energy extraction is important with regard to the magnitude of bed level change based on two main criteria: the magnitude of sediment transport at the point of extraction, and the degree of tidal asymmetry at the point of extraction. The first criterion is obvious, so the bed level change results have been normalised by the gross mean sediment transport at the point of energy extraction, averaged over the duration of the simulation (Q_T) to remove the effect of longitudinal variations in the magnitude of sediment transport at the point of energy extraction [21]. The normalised results are plotted in Fig. 7. The main finding is that when energy is extracted from a region of strong tidal asymmetry, the effect on the resulting bed level change is more pronounced (up to 29% difference from the natural tidal channel case) compared with energy extracted from regions of tidal symmetry (18% difference). For the three cases considered, this change was discernible at the bed load parting zone ($x = 78$ km) and in the region of strong tidal asymmetry ($x = 116$ km). Little change was discernible between the three cases in the region of the sediment convergence.

III. HEADLAND SAND BANK MAINTENANCE

Strong tidal flow past headlands and islands leads to the generation of large eddy systems, with an opposite sense of vorticity between the flood and ebb phases of the tide [28]. The outward-directed centrifugal force within each eddy is balanced by the inward-directed pressure gradient [29]–[31]. Since the centrifugal force is weaker at the bed (due to bed friction), this leads to the inward movement of relatively coarse sediment at the bed, leading to a convergence of sand as a function of the instantaneous eddies (Fig. 8). The sand banks which form as a result of this convergence can be up to 10 km in length [32], and so have an important role in coastal processes. Such submerged banks cause waves

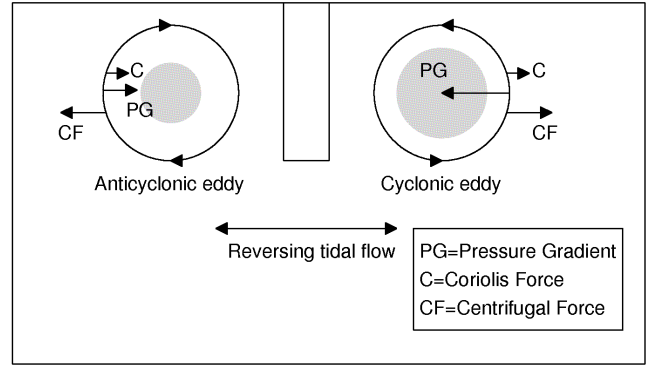


Fig. 8. Mechanism for headland sand bank formation, based on [29] and [30]. Reversing tidal flow past the headland leads to the generation of eddy systems with an opposite sense of vorticity between the flood and ebb phases of the tide. The outward-directed centrifugal force (CF) within each eddy is balanced by an inward-directed pressure gradient (PG). This leads to the inward movement of relatively coarse sediment near the bed (where the centrifugal force is weaker due to bed friction), and the formation of headland sand banks. At relatively high latitudes, the Coriolis force (C) leads to the formation of asymmetrical sand banks, with the cyclonic eddy generating a larger sand bank than the anticyclonic eddy. Grey shading indicates the location (and scale) of sand banks.

to refract and diffract, and can lead to localised regions of increased/decreased wave energy [33]–[35]. However, due to depth-induced wave breaking, the sand banks lead to an overall reduction in wave energy, and so have an important role in coastal defence [32], [36]. Offshore sand banks can be a strategic source of marine aggregates, and provide important nursery grounds for fisheries [32]. Regions of strong tidal flow past headlands and islands have been listed as potential sites for the exploitation of the tidal stream resource, such as Portland Bill in the English Channel [37], Admiralty Head in the Puget Sound [38], and flow past the island of Alderney in the Channel Islands [26]. The aim of this section is therefore to determine how such exploitation in the vicinity of headlands would affect the maintenance of the associated sand banks. This is addressed through a simple series of model experiments applied to an idealised headland configuration.

A. Two-Dimensional Morphological Model

The hydrodynamics for the headland case were generated by the three-dimensional (3D) POLCOMS model [39], formulated in spherical polar coordinates and using 20 terrain-following (σ) layers in the vertical. Neglecting the baroclinic terms and barotropic meteorological effects (e.g. wind stress and atmospheric pressure), the depth-mean POLCOMS equations of motion are [39]

$$\frac{\partial \bar{u}}{\partial t} = f\bar{v} - \frac{g}{R \cos \phi} \frac{\partial \zeta}{\partial \chi} - \frac{F_B}{H} + NL_x \quad (6)$$

and

$$\frac{\partial \bar{v}}{\partial t} = -f\bar{u} - \frac{g}{R} \frac{\partial \zeta}{\partial \phi} - \frac{G_B}{H} + NL_\phi \quad (7)$$

where \bar{u} and \bar{v} are the depth-averaged eastward and northward velocities, respectively, ζ is water surface elevation relative to mean sea level (MSL), $H = h + \zeta$ is total water depth (where

h is water depth relative to MSL), χ and ϕ are the eastwards and northwards coordinates, respectively, $f = 2\Omega \sin(\phi)$ is the Coriolis parameter (where $\Omega = 7.27 \times 10^{-5} \text{ s}^{-1}$ is the angular velocity of the Earth), R is the radius of the Earth, g is gravitational acceleration, NL_χ and NL_ϕ are the non-linear terms, and F_B and G_B are, respectively, the eastward and northward components of bed shear stress, calculated from

$$(F_B, G_B) = C_D(u_B, v_B)\sqrt{u_B^2 + v_B^2} \quad (8)$$

where u_B and v_B are the near-bed velocities, defined at a height δ above the bed, and C_D is the drag coefficient (based on an assumed logarithmic velocity profile)

$$C_D = \left(\frac{\kappa}{\ln(\delta/z_0)} \right)^2, \quad C_D \geq 0.005 \quad (9)$$

where $\kappa = 0.41$ is Von Karman's constant and z_0 is the roughness length (taken here as 10^{-3} m). After spinup, output from the hydrodynamic model was stored for each model cell every 15 minutes until completion of the simulation. The elevations and velocities output from the model were subsequently used as input to sediment transport formulae.

An additional bed friction source term was incorporated into the depth-mean POLCOMS equations (Eq. 6 and Eq. 7), with turbine characteristics parameterised from the power curve in Fig. 5. If we assume that the flow is rectilinear at the point of extraction (the ideal extraction scenario), and that the orientation of each device is optimised to make the maximum use of this flow direction, then power P (in W per device) can be calculated as a function of the magnitude of the instantaneous velocity U . Therefore, the additional friction-type terms due to energy extraction (p_x and p_y) to be added to Eq. 6 and Eq. 7 are

$$p_x = -nCp \frac{P}{\rho U A H} \cos(\theta) \quad (10)$$

and

$$p_y = -nCp \frac{P}{\rho U A H} \sin(\theta) \quad (11)$$

where n is the number of turbines per model grid cell, A is the area of each grid cell, ρ is the density of seawater, and θ is the direction of the depth-averaged current.

Total instantaneous (bedload plus suspended load) sediment transport was again calculated using the Soulsby-Van Rijn transport formulation [6]. Two-dimensional (2D) morphological development was modelled using

$$\frac{\partial z}{\partial t} = -\frac{1}{1-p} \left\{ \frac{\partial q_{t_x}}{\partial x} + \frac{\partial q_{t_y}}{\partial y} \right\} \quad (12)$$

where q_{t_i} is the total load transport of sediment in the i direction.

Eq. 12 was implemented by reading the depth-averaged velocities at 15 minute intervals as output from the hydrodynamic model. These velocities were used to calculate the instantaneous sediment transport, and this was subsequently used as input to Eq. 12 to predict bed level change (i.e the morphological timestep was 15 minutes). In each of the model

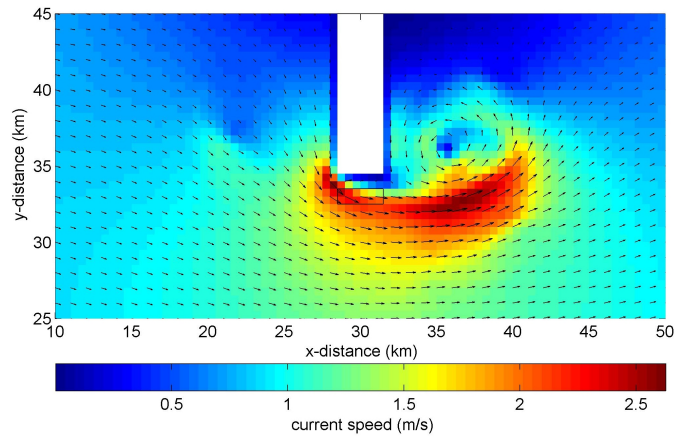


Fig. 9. Magnitude and direction of velocity around idealised headland when the flood eddy is fully developed. The box indicates the location of the TEC array.

runs, the duration of the simulation was less than one month, sufficient to examine the initial sedimentation/erosion of the bed. Since the change in bed level \ll water depth over this time period, feedback between the evolving bed (Eq. 12) and the hydrodynamic flow field was not included. Further, it was assumed that an infinite supply of sediment was available for transport.

B. Application to an Idealised Headland

A channel of length 60 km was simulated, with a width of 50 km, and a constant depth of $h = 50$ m. A headland of length 15 km and width 3 km was located mid-way along the channel (Fig. 9), a configuration which has been demonstrated to produce headland sand banks [40]. Horizontal grid spacing was $\delta x = \delta y = 500$ m, and the open boundaries were driven by a normal component of depth-averaged velocity with an amplitude of 1 m s^{-1} and period equal to the principal lunar semi-diurnal constituent (M_2). A no-slip boundary condition was applied to all coastlines. The duration of the simulations was 50 tidal cycles, sufficient to examine the initial sedimentation pattern. The highest velocities (amplitude $\sim 3.5 \text{ m s}^{-1}$) occur close to the headland and, after some trial simulations, a 3 km^2 region close to the tip of the headland was selected to site a TEC array (Fig. 9). Applying a lateral spacing of 3 turbine widths and a downstream spacing of 15 turbine widths to eliminate lateral and wake effects, respectively (e.g. [26]), a simple rectangular arrangement of 16×1.5 MW TEC devices can be accommodated within each of the 0.25 km^2 model grid cells, leading to a net (rated) TEC array of 288 MW. The sediment transport formulae were applied to a medium sand ($d_{50} = 300 \text{ }\mu\text{m}$).

C. Model Results

In the absence of artificial energy extraction (i.e the baseline case), the modelled change in bed level for the idealised headland is given in Fig. 10a. From an initial flat bed, two sand banks have evolved with a horizontal length scale of around

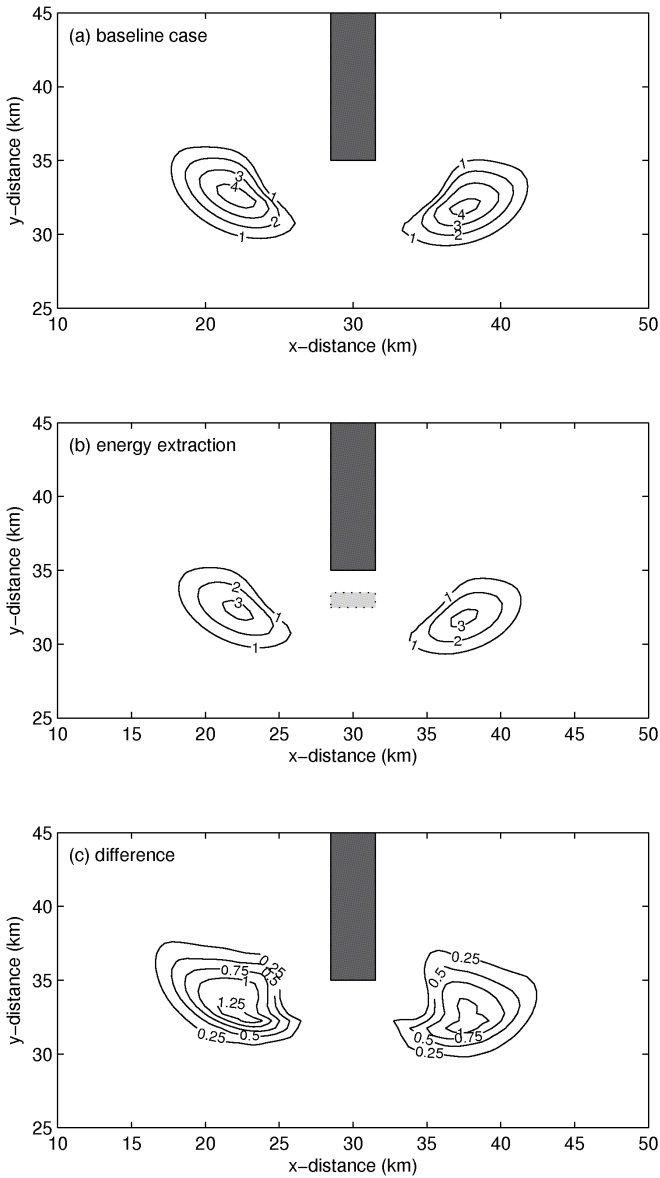


Fig. 10. Modelled dominant sand bank formation for an idealised headland using $d_{50} = 300 \mu\text{m}$. Contours (in cm) show the magnitude of deposition after 50 tidal cycles, with varying contour intervals (labelled). (a) baseline case, (b) artificial energy extraction case, and (c) difference between (a) and (b). The dark shading indicates the location of the headland, and the light shading in (b) indicates the location of the TEC array.

7 km, one located on either side of the headland. Since the duration of this morphological simulation was 50 tidal cycles, this represents the initial sedimentation pattern, rather than equilibrium, hence the change in bed level is relatively small (around 4 cm). After including the parameterisation of the 288 MW TEC array in the hydrodynamic model, the resulting sedimentation pattern is qualitatively similar, but reduced in magnitude (Fig. 10b). The difference plot makes this clear (Fig. 10c), with a reduction in magnitude of deposition at the centre of the sand banks of around 30% compared with the baseline case. Note that due to the influence of the Coriolis

force (Fig. 8) and the varying influence of friction between the flood and ebb phases of the tide (due to different water depths in the domain between flood and ebb) [31], there is slight asymmetry in sand bank formation, and hence in the influence of the TEC array. The results in Fig. 10 demonstrate that a full-scale TEC array located close to the tip of a headland could have an impact on the maintenance of the associated headland sand banks. These results suggest that TEC array developers should proceed with caution in the vicinity of headlands.

IV. DISCUSSION AND CONCLUSIONS

Results from 1D and 2D models have demonstrated that TEC array operation can have a significant impact on the morphodynamics of tidal systems. The magnitude of this impact depends upon the tidal asymmetry at the point of extraction. This supports the hypothesis presented in Section II: energy extracted from regions of strong tidal asymmetry will have a greater influence on large-scale sediment dynamics than energy extracted from regions of tidal symmetry. The resulting change in bed level was not restricted to the immediate vicinity of the TEC array, as would occur, for example, in the case of localised scour. In the model of the Bristol Channel, the change in morphodynamics due to TEC array operation was evident up to 50 km from the location of energy extraction.

Although the 1D model of the Bristol Channel demonstrates general impacts of TEC array operation on morphodynamics, the 2D headland sand bank model demonstrates more detailed impacts. Headland sand banks cause waves to refract and dissipate wave energy, and so have an important role in coastal processes, including coastal protection from storm waves. Our idealised model simulations indicate that a change in the deposition of sand on the headland sand banks of around 30% could occur during short-term TEC array operation. If the scale of this change is demonstrated to be significant compared to the natural range of inter-annual and inter-seasonal variability, then developers of TEC arrays would be advised to examine ways in which they could reduce the environmental impacts of TEC arrays sited in the vicinity of headlands.

ACKNOWLEDGEMENT

This work was undertaken within the context of the Low Carbon Research Institute Marine Consortium (www.lcri.org.uk). Simon Neill acknowledges the financial support of the Welsh Government, the Higher Education Funding Council for Wales, the Welsh European Funding Office, and the European Regional Development Fund Convergence Programme.

REFERENCES

- [1] S. J. Couch and I. G. Bryden, "Tidal current energy extraction: hydrodynamic resource characteristics," *Proc. Inst. Mech. Eng. Part M - Journal of Engineering for the Maritime Environment*, vol. 220, pp. 185–194, 2006.
- [2] S. J. Couch and I. G. Bryden, "Large-scale physical response of the tidal system to energy extraction and its significance for informing environmental and ecological impact assessment," in *Proceedings Oceans 2007 - Europe*, 2007, Vols 1-3, pp. 912-916.

- [3] The Robert Gordon University, "A scoping study for an environmental impact field programme in tidal current energy," DTI publication URN 02/882, 2002.
- [4] G. W. Boehlert and A. B. Gill, "Environmental and ecological effects of ocean renewable energy development: a current synthesis," *Oceanography*, vol. 23, pp. 68–81, 2010.
- [5] I. G. Bryden and S. J. Couch, "ME1 - marine energy extraction: tidal resource analysis," *Renew. Energ.*, vol. 31, pp. 133–139, 2006.
- [6] R. L. Soulsby, "Dynamics of marine sands," HR Wallingford, Tech. Rep. SR 466, 1997.
- [7] I. G. Bryden, "The marine energy resource, constraints and opportunities," *P. I. Civil Eng. - Mar. En.*, vol. 159, pp. 55–65, 2006.
- [8] R. D. Pingree and D. K. Griffiths, "Sand transport paths around the British Isles resulting from the M_2 and M_4 tidal interactions," *J. Mar. Biol. Assoc. U.K.*, vol. 59, pp. 497–513, 1979.
- [9] A. H. Stride, "Sediment transport by the North Sea," in *North Sea Science*, E. Goldberg, Ed. M.I.T. Press, 1973, pp. 101–130.
- [10] M. A. Johnson, N. H. Kenyon, R. H. Belderson, and A. H. Stride, "Sand transport," in *Offshore Tidal Sands, Processes and Deposits*, A. Stride, Ed. London: Chapman Hall, 1982, pp. 58–94.
- [11] A. H. Stride and R. H. Belderson, "A reassessment of sand transport paths in the Bristol Channel and their regional significance," *Mar. Geol.*, vol. 92, pp. 227–236, 1990.
- [12] C. T. Friedrichs and D. G. Aubrey, "Non-linear tidal distortion in shallow well-mixed estuaries: a synthesis," *Estuar. Coast. Shelf S.*, vol. 27, pp. 521–545, 1988.
- [13] M. R. Hashemi, M. J. Abedini, S. P. Neill, and P. Malekzadeh, "Tidal and surge modelling using differential quadrature: a case study in the Bristol Channel," *Coast. Eng.*, vol. 55, pp. 811–819, 2008.
- [14] R. J. Uncles, "Hydrodynamics of the Bristol Channel," *Mar. Pollut. Bull.*, vol. 15, pp. 47–53, 1984.
- [15] R. Kirby and T. L. Shaw, "Severn Barrage, UK - environmental reappraisal," *P. I. Civil Eng. - Engineering Sustainability*, vol. 158, pp. 31–39, 2005.
- [16] Baker C, Leach P, "Tidal lagoon power generation scheme in Swansea Bay," a report on behalf of the Department of Trade and Industry and the Welsh Development Agency, DTI publication URN 06/1051 2006.
- [17] Black & Veatch, "Tidal Stream - Phase II UK Tidal Stream Energy Resource Assessment," a report to the Carbon Trust's Marine Energy Challenge, 2005.
- [18] British Wind Energy Association, "The path to power: delivering confidence in Britain's wave and tidal stream industry," 2006.
- [19] I. S. Robinson, "Tides in the Bristol Channel - an analytical wedge model with friction," *Geophysical Journal of the Royal Astronomical Society*, vol. 62, pp. 77–95, 1980.
- [20] G. I. Taylor, "Tides in the Bristol Channel," *Proceedings of the Cambridge Philosophical Society*, vol. 20, pp. 320–325, 1921.
- [21] S. P. Neill, E. J. Litt, S. J. Couch, and A. G. Davies, "The impact of tidal stream turbines on large-scale sediment dynamics," *Renew. Energ.*, vol. 34, pp. 2803–2812, 2009.
- [22] C. A. Douglas, G. P. Harrison, and J. P. Chick, "Life cycle assessment of the Seagen marine current turbine," *Proc. Inst. Mech. Eng. Part M: Journal of Engineering for the Maritime Environment*, vol. 222, pp. 1–12, 2008.
- [23] S. P. Neill, M. R. Hashemi, and A. J. Elliott, "An enhanced depth-averaged tidal model for morphological studies in the presence of rotary currents," *Cont. Shelf Res.*, vol. 27, pp. 82–102, 2007.
- [24] J. Brown, A. E. Joyce, J. N. Aldridge, E. F. Young, L. Fernand, and P. A. Gurbutt, "Further identification and acquisition of bathymetric data for Irish Sea modelling," DETR Research Contract CW0753, Tech. Rep., 1999.
- [25] S. P. Neill, A. J. Elliott, and M. R. Hashemi, "A model of inter-annual variability in beach levels," *Cont. Shelf Res.*, vol. 28, pp. 1769–1781, 2008.
- [26] L. Myers and A. S. Bahaj, "Simulated electrical power potential harnessed by marine current turbine arrays in the Alderney Race," *Renew. Energ.*, vol. 30, pp. 1713–1731, 2005.
- [27] P. McLaren, M. B. Collins, S. Gao, and R. I. L. Powys, "Sediment dynamics of the Severn Estuary and inner Bristol Channel," *J. Geol. Soc.*, vol. 150, pp. 589–603, 1993.
- [28] I. S. Robinson, "Tidal vorticity and residual circulation," *Deep-Sea Res.*, vol. 28, pp. 195–212, 1981.
- [29] R. D. Pingree, "The formation of the Shambles and other banks by tidal stirring of the seas," *J. Mar. Biol. Assoc. U.K.*, vol. 58, pp. 211–226, 1978.
- [30] R. P. Signell and C. K. Harris, "Modeling sand bank formation around tidal headlands," in *Proceedings 6th International Conference Estuarine and Coastal Modeling, New Orleans, LA, November 1999*, M. L. Spaulding and A. F. Blumberg, Eds. ASCE Press, 2000, pp. 209–222.
- [31] S. P. Neill, "The role of Coriolis in sandbank formation due to a headland/island system," *Estuar. Coast. Shelf S.*, vol. 79, pp. 419–428, 2008.
- [32] K. R. Dyer and D. A. Huntley, "The origin, classification and modelling of sand banks and ridges," *Cont. Shelf Res.*, vol. 19, pp. 1285–1330, 1999.
- [33] J. C. W. Berkhoff, "Mathematical models for simple harmonic linear water waves," Delft Hydraulics Laboratory, Tech. Rep. Rep. W 154-IV, 1976.
- [34] A. C. Radder, "On the parabolic equation method for water-wave propagation," *J. Fluid Mech.*, vol. 95, pp. 159–176, 1979.
- [35] B. Li, D. E. Reeve, and C. A. Fleming, "Numerical solution of the elliptic mild-slope equation for irregular wave propagation," *Coast. Eng.*, vol. 20, pp. 85–100, 1993.
- [36] N. J. MacDonald and B. A. O'Connor, "Changes in wave impact on the Flemish coast due to increased mean sea level," *J. Marine Syst.*, vol. 7, pp. 133–144, 1996.
- [37] W. M. J. Batten, A. S. Bahaj, A. F. Molland, J. R. Chaplin, and Sustainable Energy Research Group, "Experimentally validated numerical method for the hydrodynamic design of horizontal axis tidal turbines," *Ocean Eng.*, vol. 34, pp. 1013–1020, 2007.
- [38] K. M. Thyng and J. J. Riley, "Idealized headland simulation for tidal hydrokinetic turbine siting metrics," in *Oceans 2010*, Sept. 2010, pp. 1–6.
- [39] J. T. Holt and I. D. James, "An s coordinate density evolving model of the northwest European continental shelf: 1 model description and density structure," *J. Geophys. Res.*, vol. 106, no. C7, pp. 14 015–14 034, 2001.
- [40] S. P. Neill and J. D. Scourse, "The formation of headland/island sandbanks," *Cont. Shelf Res.*, vol. 29, pp. 2167–2177, 2009.